Six-Channel Diplexer using Stub-Loaded Stepped Impedance Resonators

Jinlin Liu, Tao Su*, Huanhuan Lv, Lei Lin, and Bian Wu

National Laboratory of Science and Technology on Antennas and Microwaves
Xidian University, Xi'an, 710071, China
xdjinlinliu@126.com, *taosu@mail.xidian.edu.cn, lvhuanhuan4213@126.com,
linleimail@126.com, bwu@mail.xidian.edu.cn

Abstract ─ In this paper, a compact six-channel diplexer with low insertion loss and high isolation level is presented. The diplexer consists of two tri-band bandpass filters (BPFs), two meander transmission lines and hook-shaped feeding lines. The BPFs are designed based on stub-loaded stepped impedance resonators (SLSIRs). Based on even- and odd-mode (EOM) analysis of the resonator, there are two resonant modes that operate at the same frequency. For splitting the two modes, stub-stub coupling is employed here. The combination of the two BPFs is implemented by utilizing two meander transmission lines as the impedance matching network. Finally the proposed diplexer operating at 1.46/1.74/2.96 GHz (for Load 1) and 0.89/1.15/2.40 GHz (for Load 2) is fabricated and measured. A good agreement between simulated and measured results evidently validates the proposed diplexer.

Index Terms ─ Bandpass filters, six-channel diplexer, stub-loaded stepped impedance resonators, stub-stub coupling.

I. INTRODUCTION

Multiplexers with multiple passbands, low insertion loss, high isolation level and compact size attract much interest in multi-band wireless communication systems. There is an increasing demand of improving the performance of the multiplexers. To achieve this aim, many of literatures have been published to introduce research and development of the multiplexers. Stepped impedance resonator (SIR) is widely used in the design of multiplexers [1-5]. In [1], new three-way resonators using connected- and edge-coupling mechanisms are designed for diplexers. In [3], a triplexer using multiple-mode resonators is presented and the triplexer features high isolation level. In order to improve the isolation level, branch-line coupler is employed to design the diplexer in [6]. Open-loop ring resonators are studied in [7-9], which can provide good performance in designing multiplexers. A distributed coupling technique, which needs no extra matching networks, is presented for designing a quadruplexer in [9]. In [10-13], several effective methods and novel structures are presented to design multiplexers.

The goal of this work is to design a six-channel diplexer with low insertion loss and high isolation level while maintaining a compact size. Even- and odd-mode (EOM) analysis method is adopted to analysis the tri-band bandpass filters (BPFs) which is the main part of the diplexer. The BPFs are designed by stub-loaded stepped impedance resonators (SLSIRs). Utilization of SLSIRs makes the diplexer feature compact size and the high harmonics can be controlled by tuning the impedance ratio and the electrical length ratio of the resonators. The impedance matching network between the two BPFs is properly designed and hook-shaped transmission lines are employed as feeding lines to provide appropriate external coupling for the passbands of the diplexer. The proposed diplexer features low insertion loss and high isolation level with a compact size. The design process is demonstrated as follows.

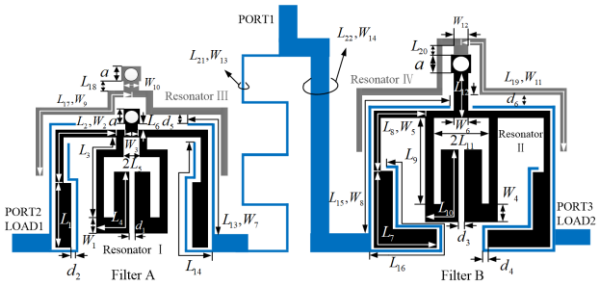

Fig. 1. Geometry of the proposed diplexer.

II. DESIGN METHODOLOGY

The geometry of the proposed diplexer consisting of two tri-band BPFs is shown in Fig. 1. Filter A is designed for Load 1 operating at 1.46/1.74/2.96 GHz and Filter B is designed for Load 2 at 0.89/1.15/2.40 GHz. The structures of two BPFs are both based on a quad-mode SLSIR (Resonator I, Resonator II) and a dual-mode SLSIR (Resonator III, Resonator IV). In this

Submitted On: January 6, 2019
Accepted On: April 3, 2019

paper, High Frequency Structure Simulation (HFSS) software with Finite Element Method (FEM) is used to analyse and optimize the performance of the proposed structure. The numerical analysis and optimization procedure is demonstrated as follows.

The equivalent structure of the SLSIR with four resonant modes (Resonator I, Resonator II) is shown in Fig. 2 (a). Because of the symmetry of the structure, EOM analysis method is used to analysis its resonant characteristics [14]. Figure 2 (b) shows the even-mode (EM) equivalent circuit of the SLSIR. Figure 2 (c) shows the odd-mode (OM) equivalent circuit of the SLSIR. As the EM and OM equivalent circuits in Fig. 2 (b) and Fig. 2 (c) are still symmetrical (L_1=L_4, L_2=L_3), EOM analysis method is used to analysis the structure again. The EOM equivalent circuits of Fig. 2 (b) are shown in Fig. 2 (d), and the EOM equivalent circuits of Fig. 2 (c) is shown in Fig. 2 (e).

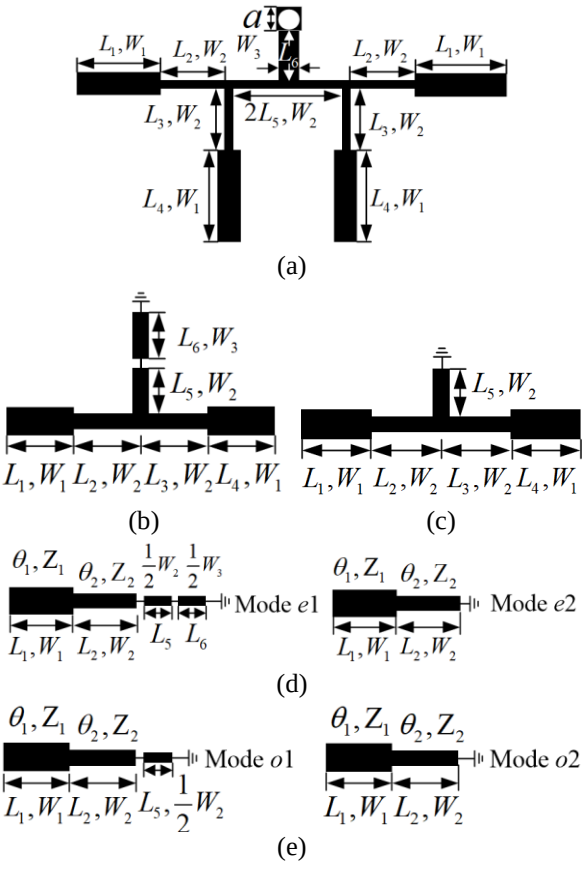

Fig. 2. (a) Schematic of the SLSIR; (b) EM equivalent circuit of the SLSIR; (c) OM equivalent circuit of the SLSIR; (d) EOM equivalent circuits of Fig. 2 (b); (e) EOM equivalent circuits of Fig. 2 (c).

It can be seen from Fig. 2 (d) and Fig. 2 (e) that there are four resonant modes in total, which are named as *e*1, *e*2, *o*1, and *o*2 respectively. It is obviously that the equivalent circuits of the four resonant modes are quarter wavelength SIRs [15]. The basic frequencies are defined as f_{e1}, f_{e2}, f_{o1} and f_{o2}. Figure 3 (a) and Fig. 3 (b) show the fundamental frequencies of four modes under different L_5 and L_6. It can be observed from Fig. 3 (a) that the variation of L_5 has an influence on f_{e1} and f_{o1}, while f_{e2} and f_{o2} remain constant. From Fig. 3 (b), it can be seen that only f_{e1} changes with the variation of L_6, while f_{e2}, f_{o1} and f_{o2} keep constant. The equivalent circuits of mode *e*2 and mode *o*2 can be considered as the basic structures of $\lambda/4$ SIR. The resonance condition can be deduced as:

$$\tan(\alpha\theta_T)\tan[(1-\alpha)\theta_T] = R_z, \quad (1)$$

$$\theta_T = \theta_1 + \theta_2, \quad (2)$$

where R_z is the impedance ratio and α is the electrical length ratio. R_z and α are defined as $R_z = Z_1 / Z_2$ and $\alpha = \theta_1 / \theta_T$ [16].

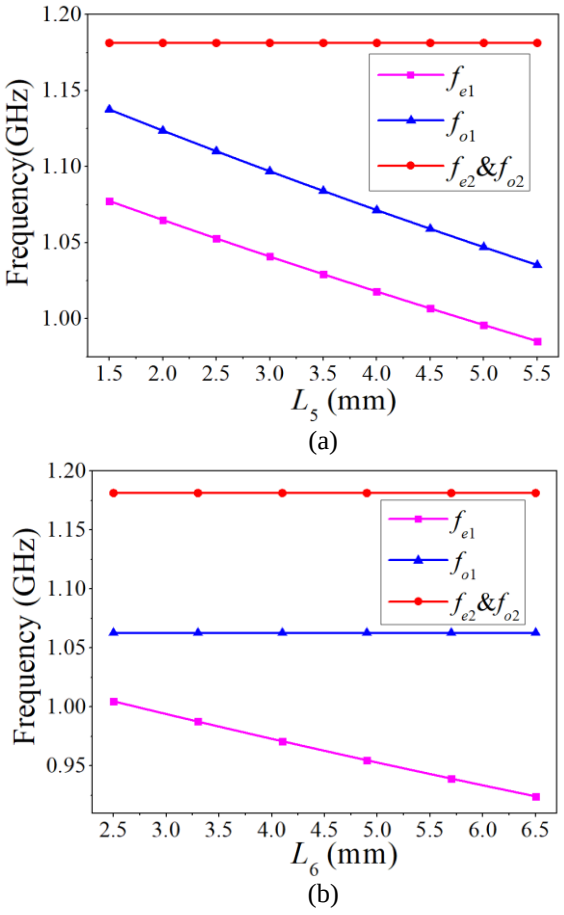

Fig. 3. Effect of (a) L_5 and (b) L_6 on fundamental frequencies of the resonant modes.

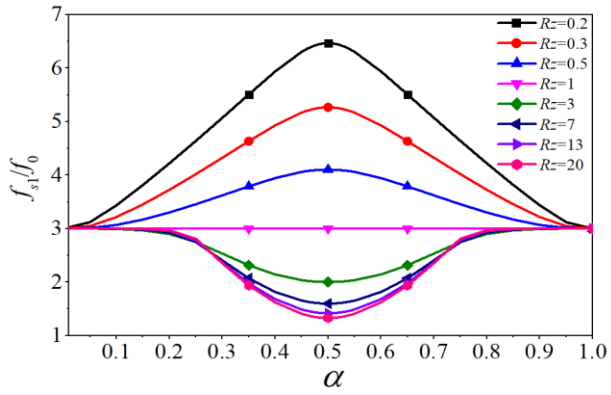

Fig. 4. Ratios of f_{s1}/f_0 with varied α and R_z.

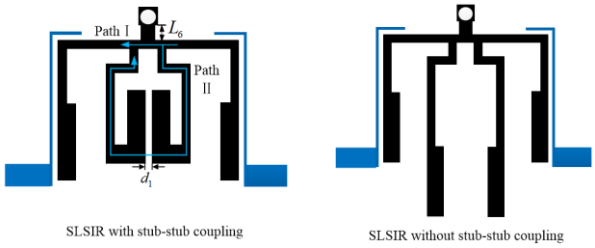

Fig. 5. SLSIR with and without stub-stub coupling.

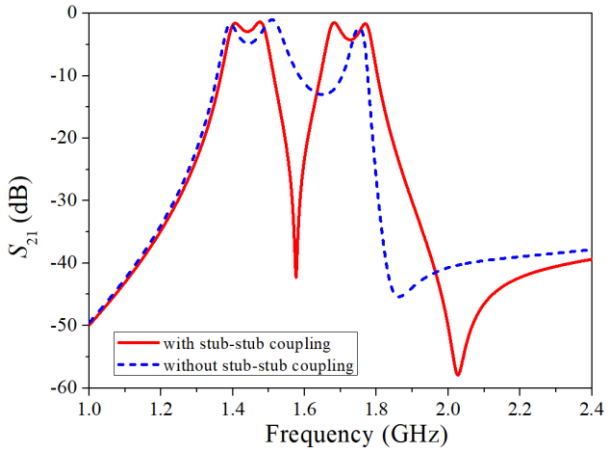

Fig. 6. Simulated results of the SLSIR with and without stub-stub coupling.

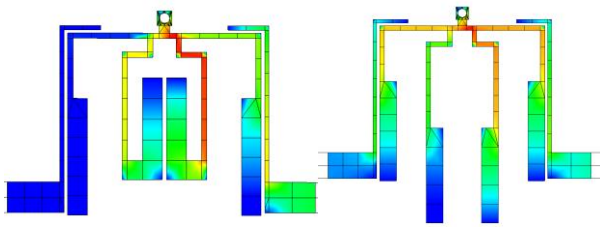

Fig. 7. Current distributions of the SLSIR at 1.58 GHz with and without stub-stub coupling.

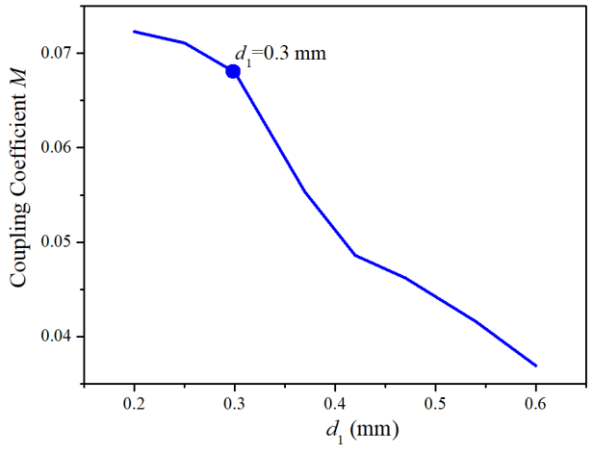

(a)

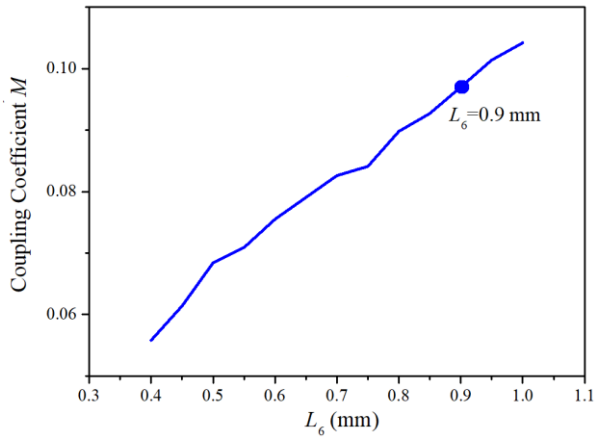

(b)

Fig. 8. (a) Simulated coupling coefficient M (for 1.74 GHz) under different d_1. (b) Simulated coupling coefficient M (for 1.46 GHz) under different L_6.

It can be seen that resonance condition of $\lambda/4$ type SIR is related to the electrical length ratio and the impedance ratio. Thus, the spurious generation can be controlled. The first harmonic frequency is defined as f_{s1} and Fig. 4 shows the relation between f_{s1}/f_0 and α with different R_z. It is obviously that frequency ratio can be configured in a wide range.

It can be seen from Fig. 2 that the equivalent circuits of Mode $e2$ and Mode $o2$ are identical. To spilt two resonant modes, we employ stub-stub coupling to introduce capacitive coupling between two stubs in the proposed SLSIR. Figure 5 shows the structure of Resonator I with and without stub-stub coupling. The resonator is folded inwards to form coupling effect, which provides additional signal deliver path. Figure 6 shows the simulated S_{21} parameter of the resonator without stub-stub coupling. By the stub-stub coupling, a transmission zero at 1.58 GHz is created. Current distributions of the resonator at the transmission zero, which are shown in Fig. 7, can be adopted here to

demonstrate the effect of stub-stub coupling. The electric current passes through the Path II due to stub-stub coupling and cancels the electric current which passes through the Path I, and this effect stimulates the transmission zero.

The coupling between the two resonant modes, which form one passband, needs to be optimized. The passband ripple is set as 0.1 dB and element values of the lowpass prototype filter are g_0=1, g_1=0.8431, g_2=0.6220 and g_3=1.3554, respectively. For the structure of Resonator I in Fig. 5, the central frequencies of the passbands are set as 1.46 GHz and 1.74 GHz. The 3 dB fractional bandwidths (FBW) is 7% and 5%, respectively. The required coupling coefficients are M=0.097 (for 1.46 GHz) and M=0.069 (for 1.74 GHz), which can be calculated theoretically from the equation:

$$M = \frac{\mathrm{FBW}}{\sqrt{g_1 g_2}}. \tag{3}$$

It is worth noting that equation (3) is used in theoretical synthesis. During the simulation and optimization, the coupling coefficients can be computed as:

$$M = \frac{f_H^2 - f_L^2}{f_H^2 + f_L^2}, \tag{4}$$

where f_H and f_L represent the higher resonant frequency and lower resonant frequency [17]. The simulated coupling coefficient at 1.46 GHz is mainly influenced by L_6 and the simulated coupling coefficient at 1.74 GHz is mainly influenced by d_1. As the length of L_6 does not influence the simulated coupling coefficient at 1.74 GHz, the value of d_1 is first decided based on the required coupling coefficient of 1.74 GHz band. Then, the value of L_6 is optimized based on the required coupling coefficient of 1.46 GHz band. Thus, the coupling coefficients of two bands can be tuned independently. Figure 8 shows the simulated coupling coefficient M under different lengths d_1 of and L_6. It can be observed that the coupling coefficient of 1.46 GHz increases with the increasing of the length of L_6, while the coupling coefficient of 1.74 GHz decreases with the increasing of the length of d_1. The optimized lengths are set as d_1=0.3 mm and L_6=0.9 mm for the required coupling coefficients. To obtain a tri-band response, we employ a dual-mode SLSIR (Resonator III), which is placed on the upper side of Resonator I as shown in Fig. 1 and operates at 2.96 GHz. Similarly, EOM method can be adopted here to make an analysis of Resonator III. The corresponding dimensions of Resonator III are optimized and a tri-band BPF Filter A can be obtained. Meanwhile, hook-shaped lines are used as feeding lines of the BPF. According to the above discussion, Filter B consisting of Resonator II and Resonator IV as shown in Fig. 1 can be designed by using the same method. The proposed diplexer is formed by the combination of Filter A and Filter B, which is implemented by utilizing two meander transmission lines as the impedance matching network.

To summarize the design procedure, design specifications are given as follows:

a) Decide the original dimensions of Resonator I and Resonator II based on the required frequencies using EOM method.

b) Calculate the required coupling coefficients, design stub-stub coupling structure and optimize the dimensions of Resonator I and Resonator II.

c) Design Resonator III and Resonator IV using EOM method.

d) Combine two BPFs by meander transmission lines and carry out final optimization of the diplexer.

III. TEST OF DIPLEXER

The thickness of the dielectric is h = 1 mm and relative permittivity of the substrate is ε_r = 2.65. The specification of the proposed diplexer is set as the center frequencies f_1=0.89 GHz, f_2=1.15 GHz, f_3=1.46 GHz, f_4=1.74 GHz, f_5=2.40 GHz, and f_6=2.96 GHz with 3 dB FBW of FBW1=11%, FBW2=9%, FBW3=7%, FBW4=5%, FBW5=4% and FBW6=3%, respectively. The required coupling coefficients are M=0.152 (for 0.89 GHz), M=0.124 (for 1.15 GHz), M=0.097 (for 1.46 GHz), M=0.069 (for 1.74 GHz), M=0.055 (for 2.40 GHz) and M=0.041 (for 2.96 GHz), respectively. The optimized dimensions are given in Table 1 (all in mm).

Table 1: Design parameters of the six-channel diplexer

PARM	Value	PARM	Value	PARM	Value
L_1	10.1	L_2	13.3	L_3	13.3
L_4	10.1	L_5	1.1	L_6	0.9
L_7	18.6	L_8	17.07	L_9	17.07
L_{10}	18.6	L_{11}	3.85	L_{12}	2.26
L_{13}	18.35	L_{14}	20.3	L_{15}	31.8
L_{16}	30.4	L_{17}	19.14	L_{18}	0.2
L_{19}	23.12	L_{20}	0.48	L_{21}	69.07
L_{22}	39.3	W_1	1.9	W_2	0.5
W_3	1	W_4	1.85	W_5	0.5
W_6	1	W_7	0.4	W_8	0.4
W_9	0.5	W_{10}	1.4	W_{11}	0.15
W_{12}	1	W_{13}	0.7	W_{14}	2.7
d_1	0.3	d_2	0.35	d_3	0.3
d_4	0.2	d_5	0.4	d_6	0.52
a	1.4				

Figure 9 shows the photograph of the fabricated diplexer. The circuit size is around $0.37\lambda_g \times 0.18\lambda_g$, where λ_g is the guide wavelength on the used substrate at 0.89 GHz.

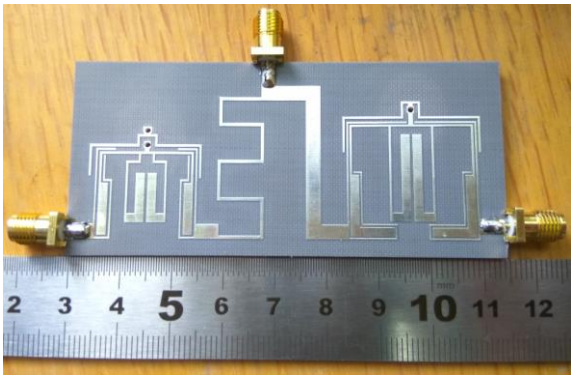

Fig. 9. Photograph of the fabricated diplexer.

Simulated and measured *S*-parameters of the proposed diplexer are shown in Fig. 10. Agilent 8719ES network analyzer is adopted here to measure the performance of the diplexer. The measured central frequencies of six channels of the diplexer locate at 0.89 GHz, 1.16 GHz, 1.46 GHz, 1.75 GHz, 2.4 GHz and 2.96 GHz with 3dB FBW of 10%, 9%, 6%, 6%, 4% and 3%, respectively. The measured minimum insertion losses of six channels are 0.95 dB, 0.84 dB, 1.3 dB, 1.17 dB, 1.57 dB and 1.8 dB, whereas the simulated minimum insertion losses are 0.72 dB, 0.77 dB, 0.95 dB, 0.81 dB, 1.21 dB and 1.58 dB, respectively. The small deviation may be caused by the fabrication machining error. The S_{11} parameters are lower than -15.6 dB and the measured S_{32} is lower than -37 dB as shown in Fig. 10.

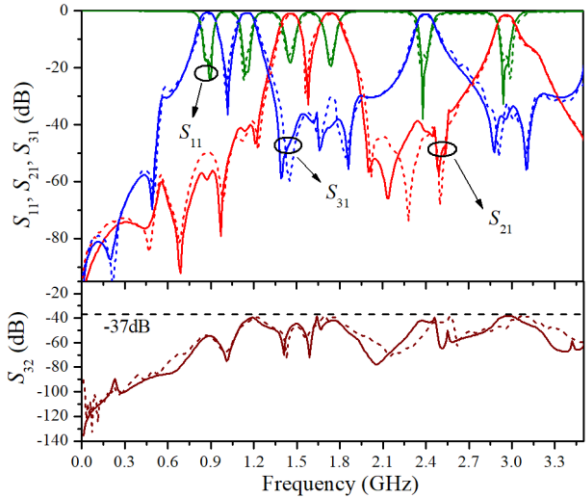

Fig. 10. Simulated and measured *S*-parameters of the proposed diplexer.

Table 2 shows comparisons between this work and previous research. It can be seen that the proposed diplexer features lower insertion loss and higher isolation with a compact size.

Table 2: Comparisons between this work and previous research

Ref.	Passbands (GHz)	Insertion Loss (dB)	Isolation (dB)	Size (λ_g^2)
6	0.9/1.5/ 2.4/3.5	2.02/1.56/ 2.08/2.52	>29	0.041
16	1.8/2.4/3.0/ 3.8/4.7/5.8	1.8/1.9/1.0/ 1.5/2.1/2.6	>30	0.057
This work	0.89/1.16/ 1.46/1.75/ 2.4/2.96	0.95/0.84/ 1.3/1.17/ 1.57/1.8	>37	0.067

IV. CONCLUSION

In this letter, a six-channel diplexer using novel SLSIRs is presented. The proposed diplexer is formed by two tri-band BPFs, which can be designed using the EOM analysis method. Two meander transmission lines are utilized to combine two BPFs and achieve impedance matching. A good agreement between simulated and measured results evidently validates the proposed diplexer.

ACKNOWLEDGMENT

This work was supported in part by the National Natural Science Foundation of China under Project 61771360 and Project 61601360, and in part by the Shaanxi Youth Science and Technology Star Project

REFERENCES

[1] S. C. Lin and T. L. Jong, "Microstrip bandpass filters with various resonators using connected- and edge-coupling mechanisms and their applications to dual-band filters and diplexers," *IEEE Trans. Microw. Theory Tech.*, vol. 60, no. 4, pp. 975-988, Apr. 2012.

[2] H. W. Liu, W. Y. Xu, Z. C. Zhang, and X. H. Guan, "Compact diplexer using slotline stepped impedance resonator," *IEEE Microw. Wireless Compon. Lett.*, vol. 23, no. 2, pp. 75-77, Feb. 2013.

[3] J. Y. Wu, K. W. Hsu, Y. H. Tseng, and W. H. Tu, "High-isolation microstrip triplexer using multiple-mode resonators," *IEEE Microw. Wireless Compon. Lett.*, vol. 22, no. 4, pp. 173-175, Apr. 2012.

[4] J. F. Chen and F. C. Chen, "Design of microstrip lowpass-bandpass quintuplexer," *Journal of Electromagnetic Waves and Applications*, vol. 30, no. 11, pp. 1474-1480, 2016.

[5] K. W. Hsu, W. C. Hung, and W. H. Tu, "Design of four-channel diplexer using distributed coupling technique," *Microwave and Optical Technology Letters*, vol. 58, no. 1, pp. 166-170, Jan. 2016.

[6] H. Sajadinia, M. Dahmardeh, and M. Khalaj-Amirhosseini, "Novel planar diplexer using branch-line coupler," *Microwave and Optical Technology Letters*, vol. 60, no. 11, pp. 2773-2777, Mar. 2018.

[7] C. M. Chen, S. J. Chang, J. C. Zheng, J. C. Liou,

and C. F. Yang, "Using folded open-loop ring resonator to design a common-mode suppression and frequency adjustable balun-bandpass filter," *Applied Computational Electromagnetics Society Journal*, vol. 31, no. 1, pp. 45-51, Jan. 2016.

[8] C. M. Chen, S. J. Chang, and C. F. Yang, "Fabrication of a novel diplexer using folded open-loop ring resonators and microstrip lines," *Applied Computational Electromagnetics Society Journal*, vol. 29, no. 11, pp. 864-869, Nov. 2014.

[9] S. J. Zeng, J. Y. Wu, and W. H. Tu, "Compact and high-isolation quadruplexer using distributed coupling technique," *IEEE Microw. Wireless Compon. Lett.*, vol. 21, no. 4, pp. 197-199, Apr. 2011.

[10] H. Chu, R. Mao, and J. X. Chen, "Development of diplexers based on dual-mode substrate integrated waveguide cavities," *Applied Computational Electromagnetics Society Journal*, vol. 32, no. 2, pp. 171-177, Feb. 2015.

[11] X. H. Guan, F. Q. Yang, H. W. Liu, and L. Zhu, "Compact and high-isolation diplexer using dual-mode stub-loaded resonators," *IEEE Microw. Wireless Compon. Lett.*, vol. 24, no. 6, pp. 385-387, June 2014.

[12] Y. X. Ji and J. Xu, "Compact BPF and diplexer using capacitively loaded λ/4 shorted meander line resonator," *Journal of Electromagnetic Waves and Applications*, vol. 28, no. 1, pp. 112-118, 2014.

[13] C. X. Zhou, Y. X. Guo, and W. Wu, "Design of lowpass filter and lowpass-highpass diplexer with LTCC technology," *Applied Computational Electromagnetics Society Journal*, vol. 31, no. 7, pp. 817-822, July 2016.

[14] T. Yang, P. L. Chi, and T. Itoh, "Compact quarter-wave resonator and its applications to miniaturized diplexer and triplexer," *IEEE Trans. Microw. Theory Tech.*, vol. 59, no. 2, pp. 260-269, Feb. 2011.

[15] F. C. Chen and Q. X. Chu, "Novel multistub loaded resonator and its application to high-order dual-band filters," *IEEE Trans. Microw. Theory Tech.*, vol. 58, no. 6, pp. 1551-1556, June 2010.

[16] Q. Li and Y. H. Zhang, "Six-channel diplexer with compact size and high isolation," *Electron. Lett.*, vol. 53, no. 17, pp. 1205-1207, Aug. 2017.

[17] Q. Li, Y. H. Zhang, and C. M. Wu, "Compact and high-isolation microstrip diplexer using distributed coupling feeding line," *Microwave and Optical Technology Letters*, vol. 60, no. 1, pp. 192-196, June 2017.